Supporting Information

One-dimensional $Ti_3C_2T_x$ MXene nanofiber anchored ultrafine iridium nanocrystals for alkaline hydrogen evolution

Xuanyin Li[a#], Zhi Qing[a#], Olim Ruzimuradov[c], Shiying Chang[d], Dong Fang[*a], Lang Zhang[*a], and Shichun Mu[*b]

[a]Advanced Power Materials Innovation Team, Faculty of Materials Science and Engineering, Kunming University of Science and Technology, Kunming, 650093, P. R. China. E-mail: fangdong@kmust.edu.cn; 3086818048@qq.com. #These authors contributed equally to this work.

[b]State Key Laboratory of Advanced Technology for Materials Synthesis and Processing, Wuhan University of Technology, Wuhan, 430070, P. R. China. E-mail: msc@whut.edu.cn

[c]Turin Polytechnic University in Tashkent, 100095 Tashkent, Uzbekistan.

[d]Yunnan Precious Metals Lab Co., Ltd., Kunming, Yunnan 650106, P. R. China.

Experimental Details

Chemical and reagents

All chemicals have reached analytical grade purity and are ready for use without further processing. MAX (Ti_3AlC_2) was purchased from 11 Technology Co., Ltd. $H_2IrCl_6 \cdot xH_2O$ from Yunnan Hongsheng Platnum Co., Ltd. Potassium Hydroxide (KOH), Hydrofluoric Acid (HF), Ethanol and commercial Ir@C catalyst were purchased from Shanghai Macklin biochemical Co., Ltd.

Materials synthesis

Synthesis of $Ti_3C_2T_x$ MXene-NS: A 40 ml of 10 wt% HF solution was added to a Teflon beaker and stirred for 2 min to obtain a homogeneous etching solution. Then, 2 g of Ti_3AlC_2 MAX phase powder was slowly added to the solution under magnetic stirring. The mixture was magnetically stirred in an oil bath at 40 ℃ for 24 h. The resulting mixture was transferred to a 50 ml centrifuge tube and washed several times with deionized water until the supernatant appeared dark green, and the pH of the supernatant was approximately 6. Each wash was performed by centrifugation at 3500 rpm for 3 min. The washed precipitate was then redispersed in 30 ml of deionized water, transferred to a gas-washing bottle, and purged with argon gas for 5 min to prevent oxidation during the delamination process. The mixture was then ultrasonicated for 2 h in an ice bath. The resulting suspension was centrifuged at 3500 rpm for 30 min, and the dark green colloidal suspension was collected and freeze-dried for 48 h to obtain etched $Ti_3C_2T_x$ MXene-NS.

Synthesis of $Ti_3C_2T_x$ MXene-NF: An appropriate amount of KOH was added to deionized water to prepare a 6 M KOH solution. In an oil bath at 35 ℃, 100 mg of the previously prepared MXene-NS was added to 200 ml 6 M KOH solution and stirred continuously for 96 h. The mixture was transferred to a 50 ml centrifuge tube and washed several times with deionized water until the pH of the supernatant was approximately 6. Each wash was performed by centrifugation at 6000 rpm for 3 min. The resulting dispersion was freeze-dried for 48 h to collect the MXene-NF.

Synthesis of Ir@NF 550 Catalyst: 10 mg of MXene-NF powder was dispersed in 800

μl of deionized water under continuous stirring to obtain an MXene-NF suspension. $H_2IrCl_6 \cdot xH_2O$ was used as the metal precursor to be loaded on MXene-NF by incipient-wetness impregnation method. 200 μL of H_2IrCl_6 solution (C = 12.5 mg mL^{-1}) was added dropwise to the MXene-NF suspension, followed by freeze-drying for 48 h. The fresh mixture was reduced under 5% H/Ar, flow at different temperatures (650 ℃, 750 ℃ and 850 ℃) for 0.5 h with a ramping rate of 5 ℃ min^{-1} to produce 4.1 wt% Ir@NF 550, Ir@NF 650 and Ir@NF 750 catalysts.

Synthesis of Ir@NF xh Catalyst: The synthesis of Ir@NF xh is almost as same as Ir@NF 550 except that holding time was extended to 1h to prepare Ir@NF 1h and extended to 2h to prepare Ir@NF 2h.

Electrochemical Measurements

All the electrochemical measurements were carried out on an electrochemical workstation (CS350M, CORRTEST) in a standard three-electrode system at room temperature. The carbon paper (0.5 cm × 1 cm) loaded with catalysts was used as the working electrode, while a Hg/HgO electrode and an unused graphited rod were used as reference electrode and counter electrode, respectively, and 1 M KOH (pH = 14) was used as the electrolytes. The catalyst ink was prepared by mixing 5 mg of catalyst, 95 μL of ethanol, and 5 μl of Nafion solution (5 wt%) followed by ultrasonication until a homogeneous suspension was obtained. Then, 10 μl of the catalysts' ink was then carefully drop-cast onto the carbon paper (0.5 cm × 0.5 cm).

For HER tests, linear sweep voltammetry (LSV) with iR-correction was carried out at a scan rate of 5 mV s^{-1}. Before LSV testing, cyclic voltammetry (CV) was performed at a scan rate of 100 mV s^{-1} for 10 cycles to stabilize the catalysts. Tafel slope was calculated based on LSV curves. The whole test data were converted to the reversible hydrogen electrode (RHE) according to the Nernst equation: E(RHE) = E(Hg/HgO) + 0.059 × pH + 0.0977. Electrochemical impedance spectroscopy (EIS) tests were performed from 100 kHz to 0.1 Hz at the overpotential of 10 mA cm^{-2}. The double-layer capacitance (C_{dl}) was used to estimate the electrochemically active surface area (ECSA). CV was also performed in the scan rate from 20 to 100 mV s^{-1} for the

double layer capacitance (C_{dl}) calculation. Cycling stability was assessed by CV conducted between 0.3 V and -0.1 V vs RHE at 100 mV s^{-1}. Chronopotentiometry measurements were recorded at a current density of 10 mA cm^{-2} for 20 h.

The TOF values can be calculated based on the following equation:

$$TOF_{HER} = \frac{j \times A}{2 \times n \times F}$$

Where j is the current density at an overpotential of 100 mV during the LSV measurement in 1.0 M KOH solution. A stand for the area of the electrode is 0.25 cm^2 and F is the Faradaic constant (96485 C mol^{-1}). 2 accounts for the electrons consumed to form H2 molecule from water ($2e^-$ for HER), n represents the number of active sites. We calculated all the noble metals on the catalyst as the catalytic active site, and the the noble metal mass was calculated from the ICP-OES results.

Materials characterization

The microstructure was characterized with field emission scanning electron microscopy (SEM) of a Sigma 300 from ZEISS. Transmission electron microscopy (TEM), High-resolution transmission electron microscopy (HRTEM), and high-angle annular dark-field scanning transmission electron microscopy (HAADF-STEM) images obtained with a FEI Talos F200X. XPS measurements were conducted using a Thermo Scientific K-Alpha X-ray photoelectron spectrometer. Inductively coupled plasma-mass spectrometry (ICP-MS) was conducted using an Agilent 5110. Raman measurements were conducted using a Renishaw invia.

DFT calculations

The density functional theory (DFT) calculations were carried out with the VASP code.[1] The Perdew–Burke–Ernzerhof (PBE) functional within generalized gradient approximation (GGA)[2] was used to process the exchange–correlation, while the project augmented-wave pseudopotential (PAW)[3] was applied with a kinetic energy cut-off of 450 eV, which was utilized to describe the expansion of the electronic eigenfunctions. The Brillouin-zone integration was sampled by a Γ-centered 5 × 5 × 1 Monkhorst–Pack

k-point. All atomic positions were fully relaxed until energy and force reached a tolerance of 1 × 10-6 eV and 0.01 eV/Å, respectively. The dispersion corrected DFT-D method was employed to consider the long-range interactions.[4]

The Gibbs free energy change (ΔG) was calculated by computational hydrogen electrode (CHE) model as follows:

$$\Delta G = \Delta E + \Delta ZPE - T\Delta S$$

where ΔE is the reaction energy obtained by the total energy difference between the reactant and product molecules absorbed on the catalyst surface and ΔS is the change in entropy for each reaction, ΔZPE is the zero-point energy correction to the Gibbs free energy. T represents room temperature (298.15 K).

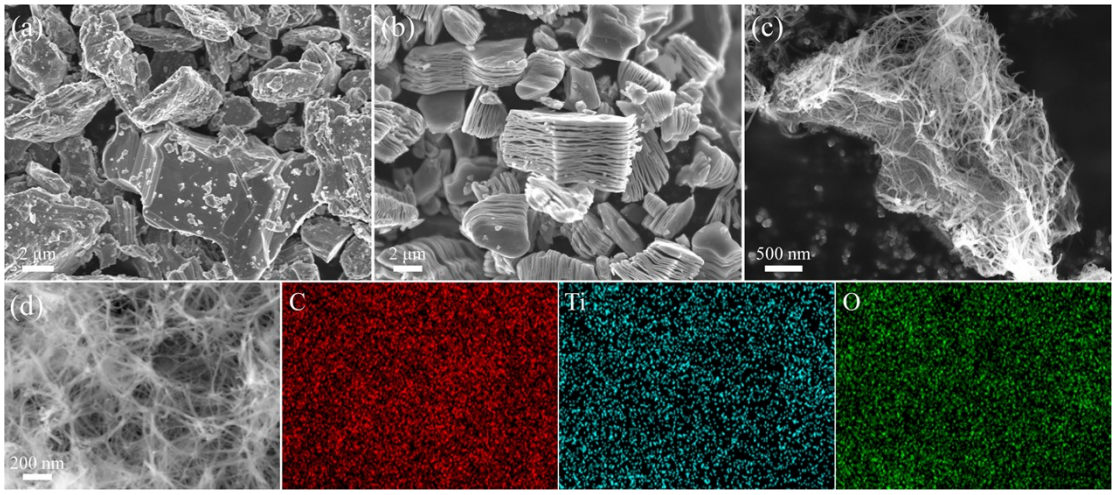

Fig. S1 SEM images of (a) MAX, (b) MXene-NS and MXene-NF; (e) SEM-EDS elemental mapping images of MXene-NF.

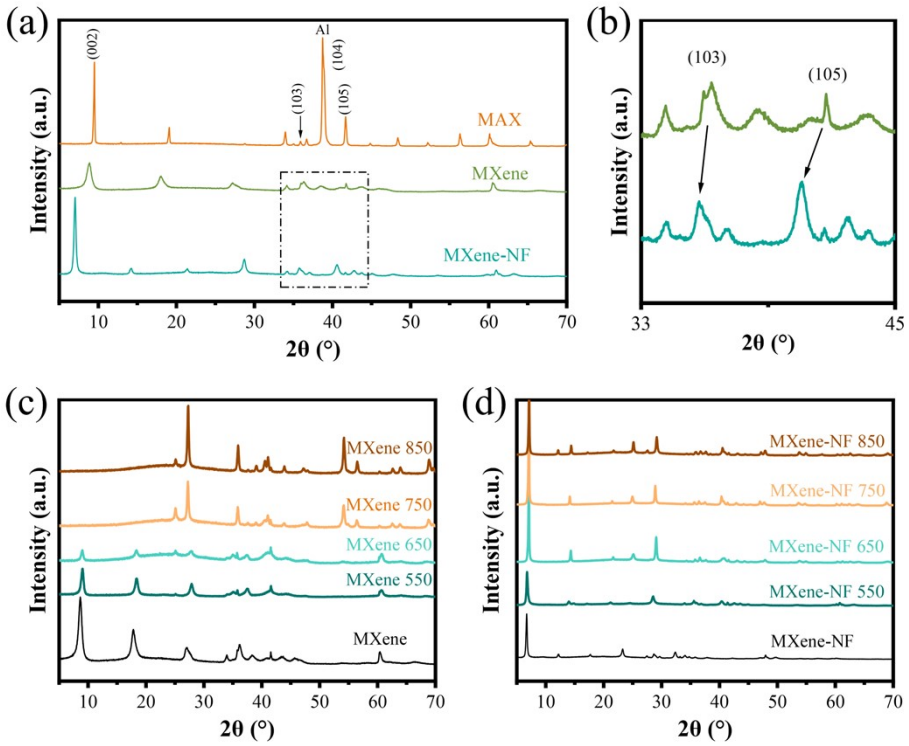

Fig. S2 XRD patterns: (a) MAX, MXene, and MXene-NF; (b) Magnified XRD patterns showing the 2θ region from (a); (c) MXene heated to different peak temperatures; (d) MXene-NF heated to different peak temperatures.

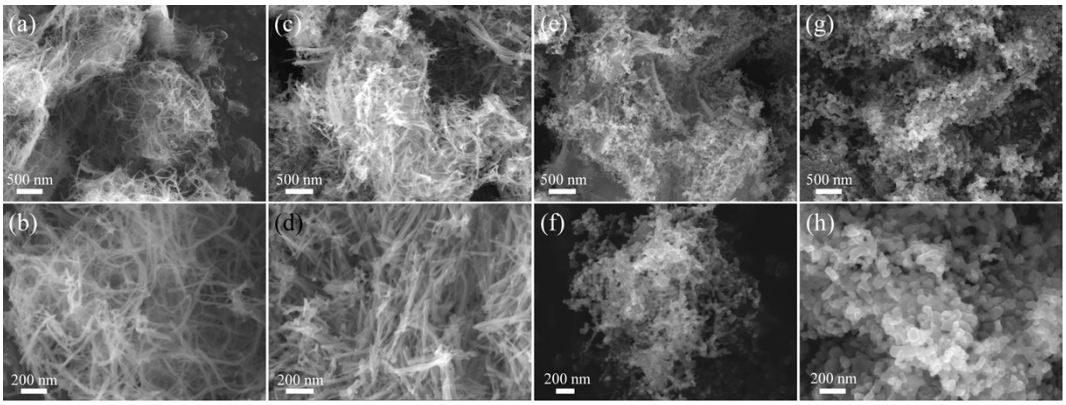

Fig. S3 SEM images of MXene-NF heated to different peak temperatures. (a, b) MXene-NF 550; (c, d) MXene-NF 650 ;(e, f) MXene-NF 750 ;(g, h) MXene-NF 850.

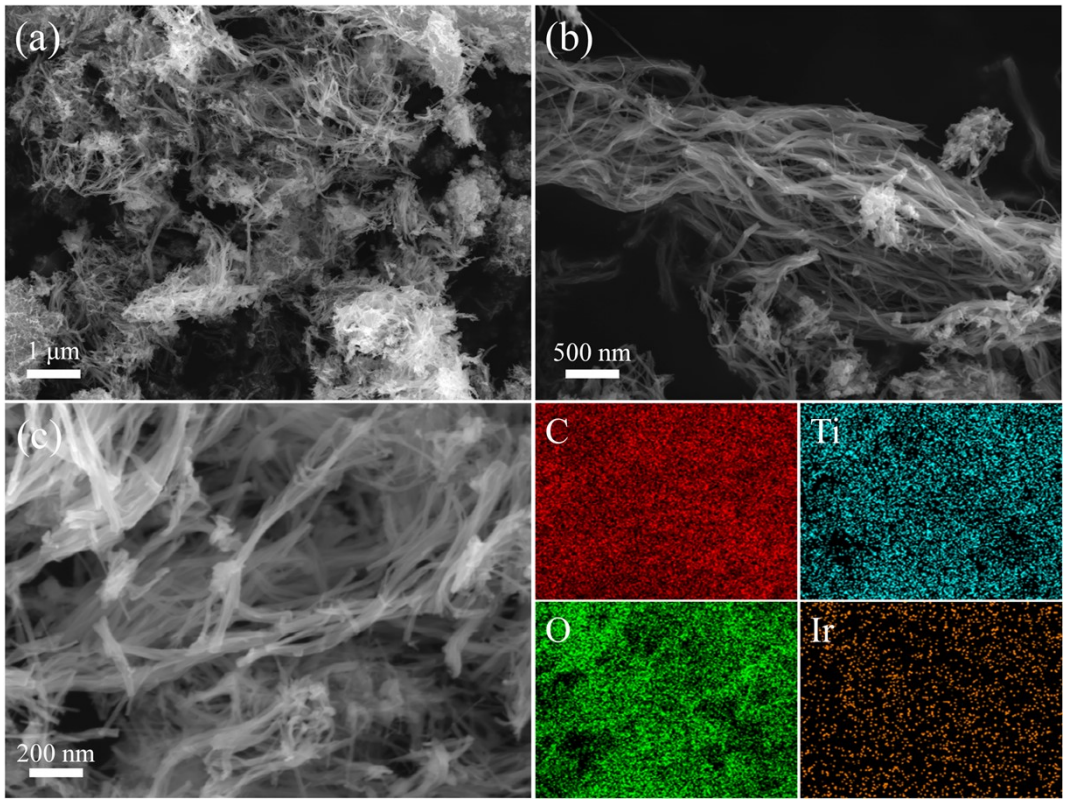

Fig. S4 SEM images of Ir@NF 550: (a) 1μm, (b) 500 nm and (c) SEM-EDS elemental mapping, 200 nm.

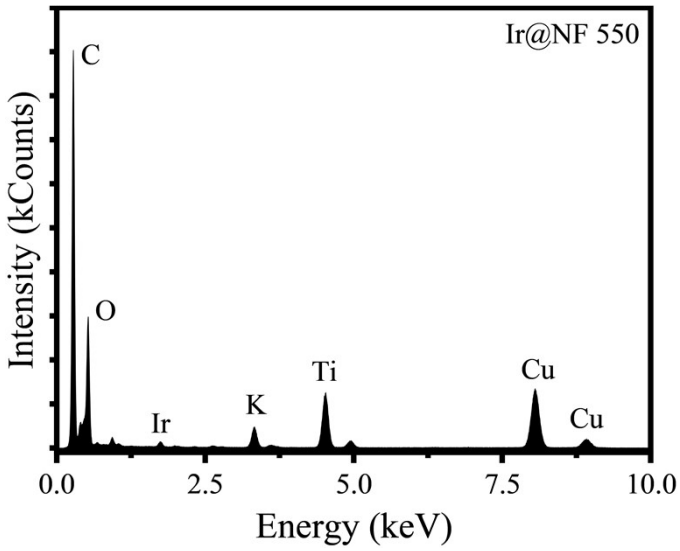

Fig. S5 The EDS composition of Ir@NF 550.

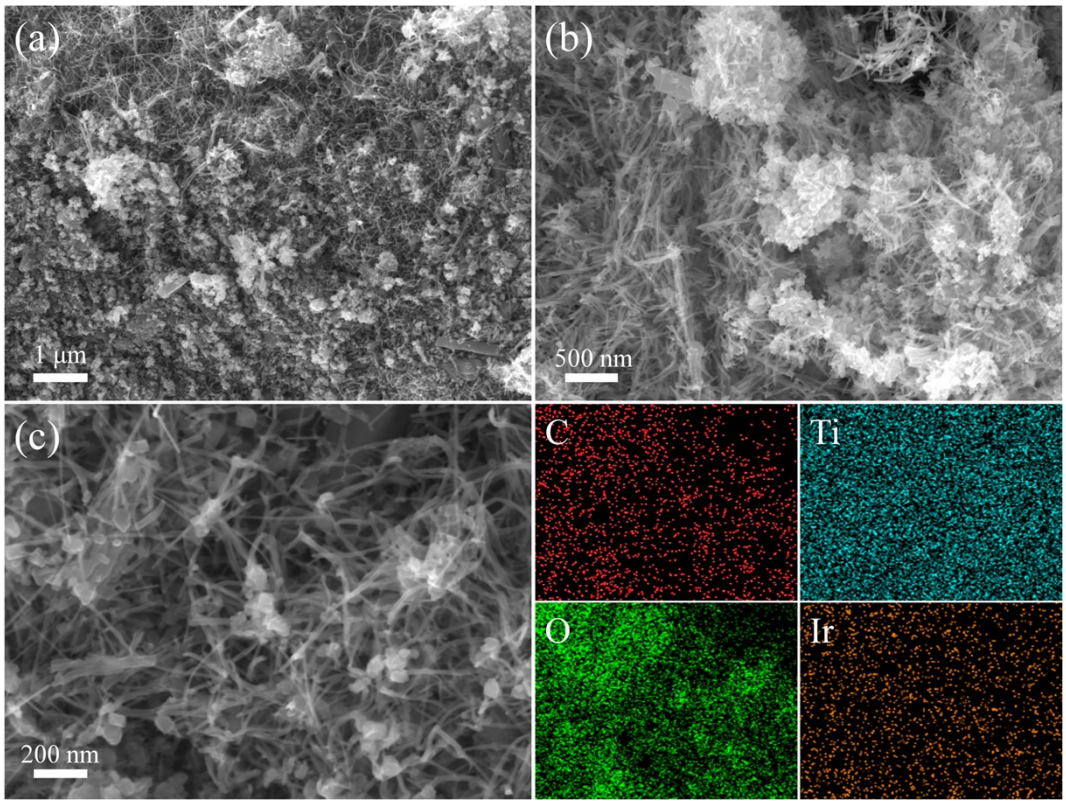

Fig. S6 SEM images of Ir@NF 650: (a) 1μm, (b) 500 nm and (c) SEM-EDS elemental mapping, 200 nm.

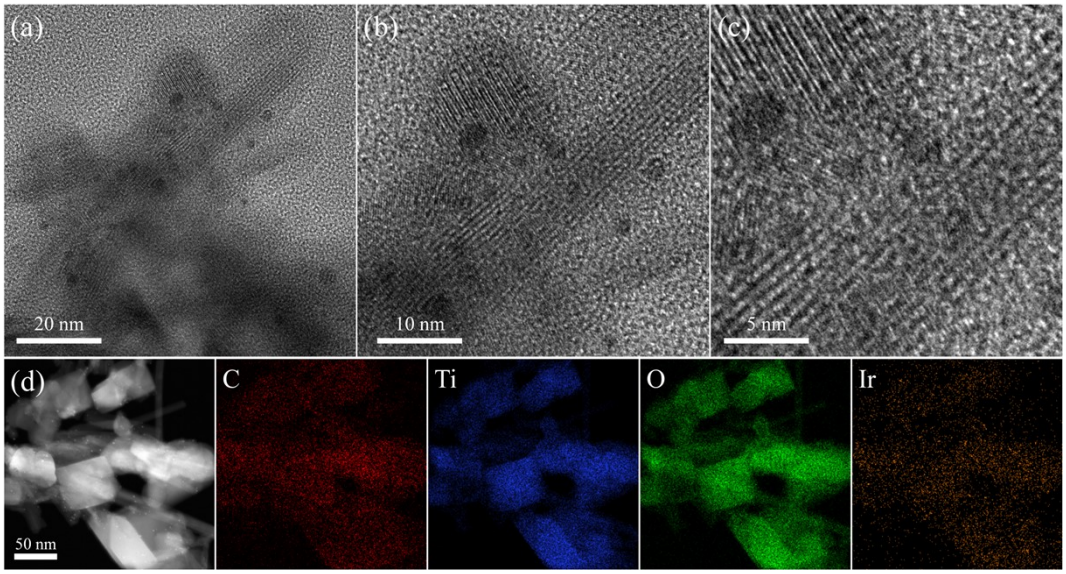

Fig. S7 HRTEM images of Ir@NF 650: (a) 20 nm, (b) 10 nm and (c) 5 nm; (D) TEM-EDS elemental mapping images, 50 nm.

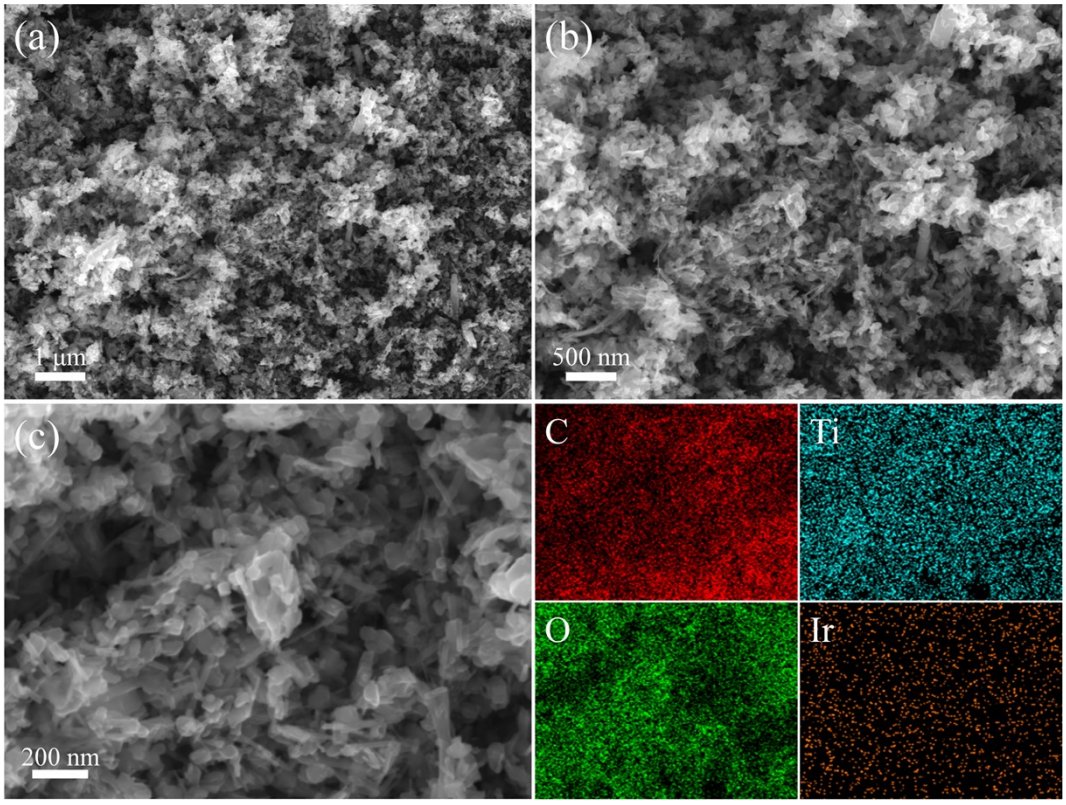

Fig. S8 SEM images of Ir@NF 750: (a) 1μm, (b) 500 nm and (c) SEM-EDS elemental mapping, 200 nm.

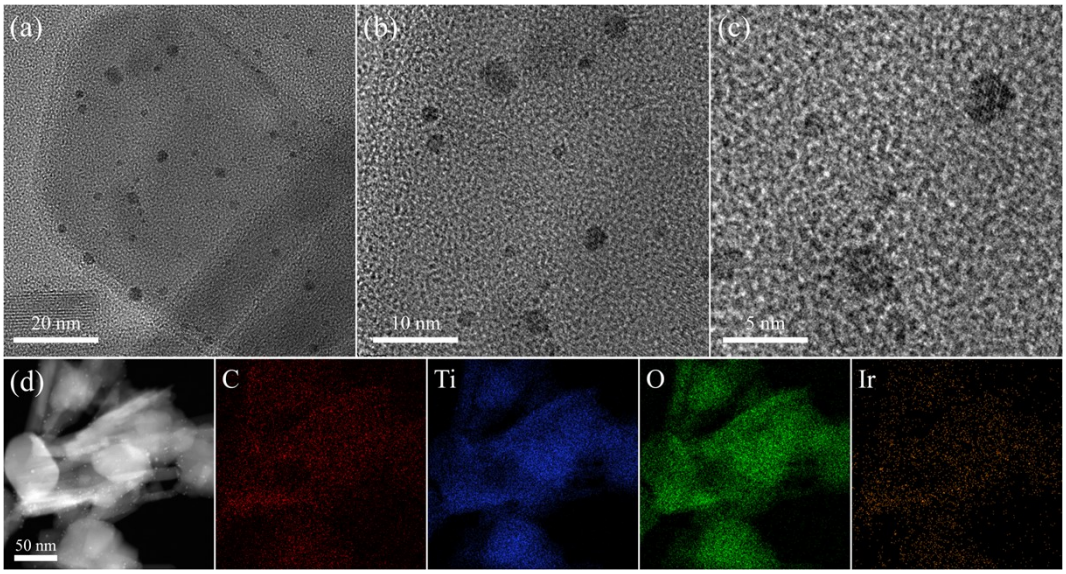

Fig. S9 HRTEM images of Ir@NF 750: (a) 20 nm, (b) 10 nm and (c) 5 nm; (D) TEM-EDS elemental mapping images, 50 nm.

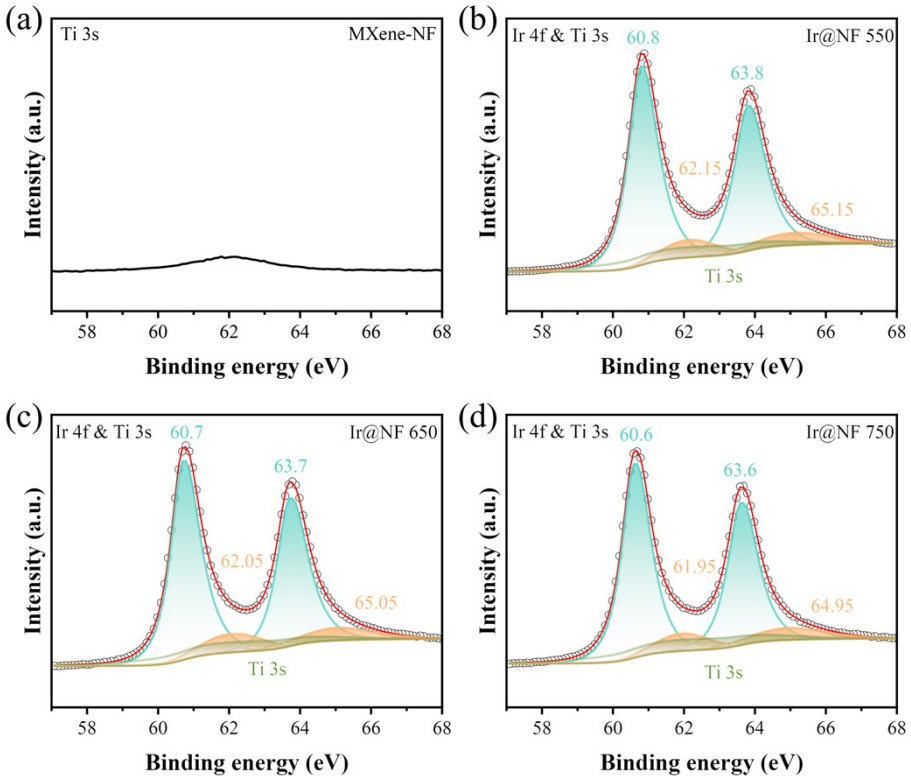

Fig. S10 high-resolution spectra of Ir 4f & Ti 3s for (a) MXene-NF, (b) Ir@NF 550, (c) Ir@NF 650 and (d) Ir@NF 750. (Normalized on the vertical scale)

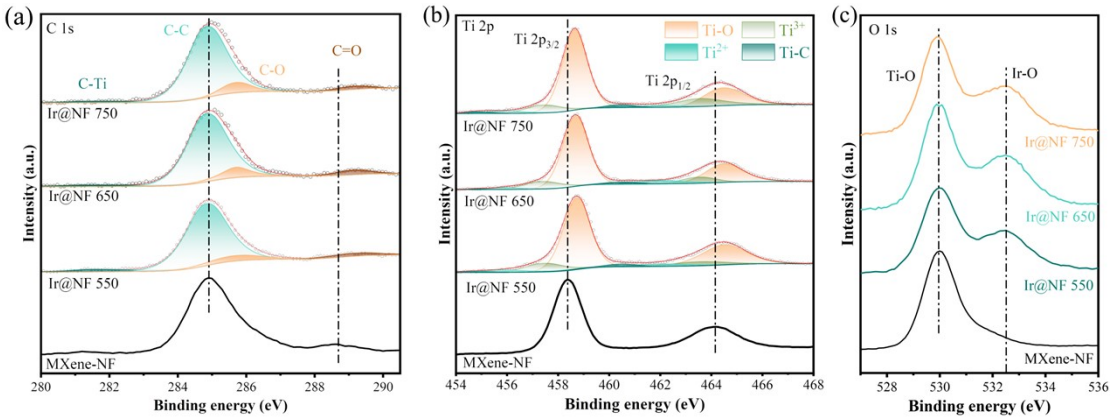

Fig. S11 high-resolution XPS spectra for MXene-NF, Ir@NF 550, Ir@NF 650 and Ir@NF 750 catalysts: (a) C 1s; (b) Ti 2p; (c) O 1s.

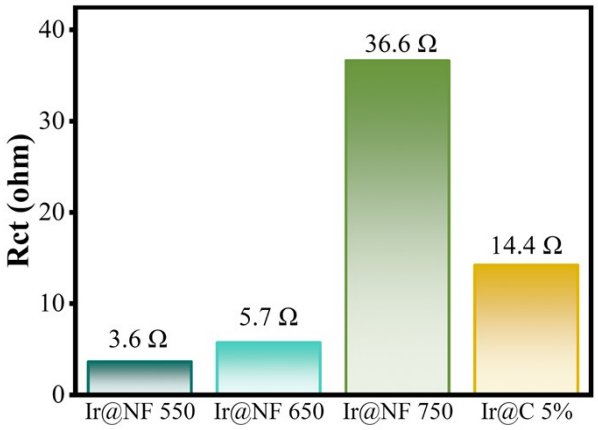

Fig. S12 Corresponding R_{ct} values of Ir@NF 550, Ir@NF 650, Ir@NF 750 and commercial Ir@C 5%.

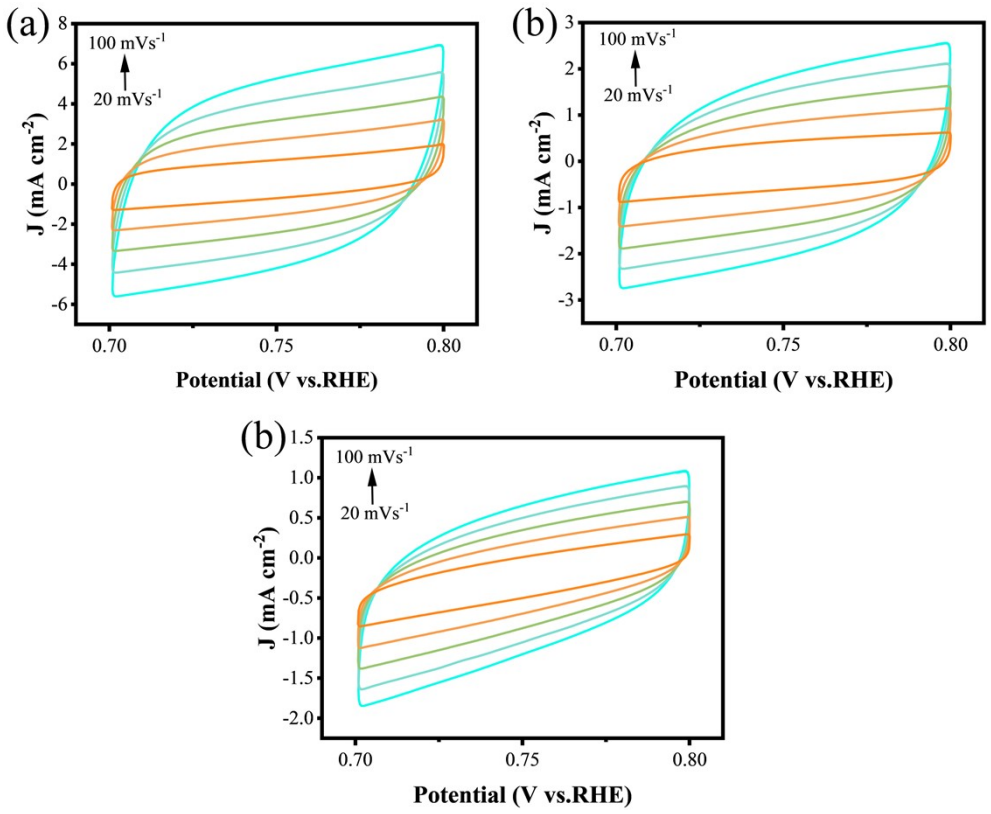

Fig. S13 CV curves at different scan rates in 1M KOH for HER of (a) Ir@NF 550, (b) Ir@NF 650 and (c) Ir@NF 750.

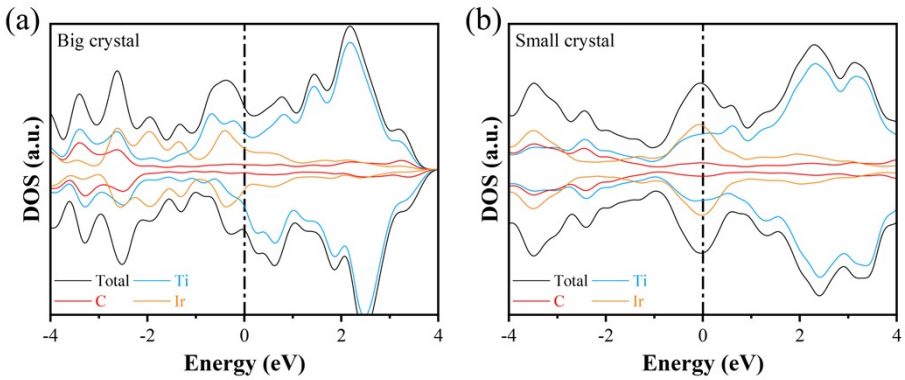

Fig. S14 DOS of (a) Big crystal and (b) Small crystal.

Table. S1 Comparison of recent reported catalysts for HER in 1M KOH.

Catalysts	Overpotential (mV) @10 mA cm^{-2}	Tafel slope (mV dec^{-1})	Refs.
Ir@NF 550	15.8	23.0	This work
Ir/$Mo_2TiC_2T_x$-750	13	20	5
Ir_{SA}-2NS-$Ti_3C_2T_x$	40.9	50.5	6
Ir/IrO_2@(N,S)-C	63	40.05	7
IrPdPb WNNs	21	66	8
Ir-NR/C	42	35.2	9
RhIr NSs/NF	15	67	10
Ir–Ni_2P/CPDs	25	31	11
ED Ir	25	34	12
Ir_2Ni_8/NHCSs	54	60	13
Ir cluster@CoO/CeO_2	54	91	14
Ir_3V/C-1000	9	24.1	15
N-PdIr bimetallene	34	81.9	16

1. G. Kresse and J. Furthmüller, Efficiency of ab-initio total energy calculations for metals and semiconductors using a plane-wave basis set, *Comput. Mater. Sci*, 1996, **6**, 15-50.
2. J. P. Perdew, K. Burke and M. Ernzerhof, Generalized Gradient Approximation Made Simple, *Phys. Rev. Lett.*, 1996, **77**, 3865-3868.
3. P. E. Blöchl, Projector augmented-wave method, *Physical Review B*, 1994, **50**, 17953-17979.
4. S. Grimme, Semiempirical GGA-type density functional constructed with a long-range dispersion correction, *J. Comput. Chem.*, 2006, **27**, 1787-1799.
5. L. Dai, Y. Shen, J. Z. Chen, L. Zhou, X. Wu, Z. Li, J. Wang, W. Huang, J. T. Miller, Q. Wang, A. Cao and Y. Wu, MXene-Supported, Atomic-Layered Iridium Catalysts Created by Nanoparticle Re-Dispersion for Efficient Alkaline Hydrogen Evolution, *Small*, 2022, **18**, 2105226.
6. W. Lin, Y.-R. Lu, W. Peng, M. Luo, T.-S. Chan and Y. Tan, Atomic bridging modulation of Ir–N, S co-doped MXene for accelerating hydrogen evolution, *J. Mater. Chem. A*, 2022, **10**, 9878-9885.
7. L. Zeng, Y. Zhu, D. Wu, H. Cheng and Q. Zhou, Cr selectively incorporated N, S-doped carbon layer encapsulating Ir/IrO2 for efficient alkaline hydrogen and oxygen evolution, *J. Alloys Compd.*, 2025, **1010**, 177371.
8. R.-L. Zhang, J.-J. Duan, L.-P. Mei, J.-J. Feng, P.-X. Yuan and A.-J. Wang, Facile synthesis of porous iridium-palladium-plumbum wire-like nanonetworks with boosted catalytic performance for hydrogen evolution reaction, *J. Colloid Interface Sci.*, 2020, **580**, 99-107.
9. F. Luo, L. Guo, Y. Xie, J. Xu, K. Qu and Z. Yang, Iridium nanorods as a robust and stable bifunctional electrocatalyst for pH-universal water splitting, *"Appl. Catal., B"*, 2020, **279**, 119394.
10. M.-T. Chen, R.-L. Zhang, J.-J. Feng, L.-P. Mei, Y. Jiao, L. Zhang and A.-J. Wang, A facile one-pot room-temperature growth of self-supported ultrathin rhodium-iridium nanosheets as high-efficiency electrocatalysts for hydrogen evolution reaction, *J. Colloid Interface Sci.*, 2022, **606**, 1707-1714.
11. D. Yue, T. Feng, Z. Zhu, S. Lu and B. Yang, Ir Single Atom-Doped Ni2P Anchored by Carbonized Polymer Dots for Robust Overall Water Splitting, *ACS Catal.*, 2024, **14**, 3006-3017.
12. L. Ju, Y. Zhang, Y. Zhou and W. Wu, Structure and performance of iridium electrocatalysts for hydrogen evolution reaction obtained by electrodeposition and double glow plasma: A comparative study, *Mater. Lett.*, 2023, **352**, 135127.
13. N. Wei, M. Mao, J. Wu, Y. Long and G. Fan, Void confinement and doping-modulation of IrNi alloy nanoparticles on hollow carbon spheres for efficient hydrogen oxidation/evolution reactions, *Fuel*, 2022, **319**, 123637.
14. L. Zhang, Y. Lei, Y. Yang, D. Wang, Y. Zhao, X. Xiang, H. Shang and B. Zhang, High Coverage Sub-Nano Iridium Cluster on Core–Shell Cobalt-Cerium Bimetallic Oxide for Highly Efficient Full-pH Water Splitting, *Adv. Sci.*, 2024, **11**, 2407475.
15. L.-W. Chen, X. Guo, R.-Y. Shao, Q.-Q. Yan, L.-L. Zhang, Q.-X. Li and H.-W. Liang, Structurally ordered intermetallic Ir3V electrocatalysts for alkaline hydrogen evolution reaction, *Nano Energy*, 2021, **81**, 105636.
16. Q. Mao, K. Deng, W. Wang, P. Wang, Y. Xu, Z. Wang, X. Li, L. Wang and H. Wang, N-doping induced lattice-strained porous PdIr bimetallene for pH-universal hydrogen evolution electrocatalysis, *J. Mater. Chem. A*, 2022, **10**, 8364-8370.